48th AIAA Aerospace Sciences Meeting Including the New Horizons Forum and Aerospace Exposition
4 - 7 January 2010, Orlando, Florida

AIAA 2010-1013

Toward Zero Sonic Boom and High Efficiency Supersonic Flight, Part I: A Novel Concept of Supersonic Bi-Directional Flying Wing

Gecheng Zha*, Hongsik Im †, Daniel Espinal‡
Dept. of Mechanical and Aerospace Engineering
University of Miami
Coral Gables, FL 33124
e-mail: gzha@miami.edu

Abstract

This paper introduces a novel concept for supersonic airplane: supersonic bi-directional (SBiDir) flying wing (FW) concept, which is to achieve low sonic boom, low supersonic wave drag, and high subsonic performance. The SBiDir-FW planform is symmetric about both longitudinal and span axes. For supersonic flight, the planform will have low aspect ratio and high sweep angle to minimize wave drag. For subsonic mode, the airplane will rotate 90° and the sweep angle will be reduced and the aspect ratio will be increased. To minimize sonic boom, the pressure surface of the flying wing will employ an isentropic compression surface. At zero angle of attack (AoA) as the example studied in this paper, a flat pressure surface achieves this purpose. The CFD simulation shows that it obtains low ground sonic boom overpressure of 0.3psf with $L/D_p = 5.3$. Furthermore, the ground pressure signature is not the N shape wave with two strong shock wave pulses, but is in a smooth *sin* wave shape. The results show that it is possible to remove or achieve very low sonic boom using a supersonic bi-directional flying wing or blended wing body configuration. Future work will optimize the SBiDir-FW concept to achieve high aerodynamic efficiency and maintain low sonic boom.

1 Introduction

Supersonic commercial flight has always been a great interest of aircraft design engineers, scientists, and business professionals due to the potential to reduce inter-continental travel time. The Concorde, the first supersonic civil transport to carry passengers, ceased service in 2003 due to high operating costs. The prohibition of the Concorde's flight over populous land areas limited its commercial success. Since the Concorde's last flight, efforts to make supersonic commercial flight economically and environmentally viable continues.

Supersonic transports (SSTs) have two major problems: efficiency and noise. The first factor that affects efficiency is the extra drag contribution during supersonic flight: the wave drag caused by the entropy increase of strong shock waves. Wave drag does not exist for subsonic airplanes and is not a serious problem for transonic flight due to the low supersonic Mach number. The second

* Ph.D., Associate Professor, Director of Aerodynamics and CFD Lab
† Ph.D. Candidate
‡ Senior undergraduate student

Copyright © 2010 by the authors of this paper. Published by the American Institute of Aeronautics and Astronautics, Inc., with permission.

factor that affects efficiency is the large flight speed disparity between take-off/landing and cruise. At take-off and landing, the low flight speed requires a high aspect ratio and low wing sweep angle. High-speed cruise however requires the opposite characteristics. A compromise between low speed take-off/landing and high-speed cruise efficiency is required. Noise is an issue caused by the sonic boom that propagates to the ground from the shock waves created by a supersonic airplane and its components. Plotkin and Maglieri[1] gave an overview of the sonic boom research on the state of the art and the problems that need to be solved.

The flying wing and blended wing body concepts eliminate the non-lifting fuselage component of the conventional tube and wing configuration, so efficiency during subsonic flight is improved. However, the flight of a supersonic flying wing or blended wing body configuration for civil transport has not appeared, and the full conceptual study of such configurations is rarely seen. The oblique flying wing (OFW) concept first proposed by Jones was intended for the development of supersonic flying wings[2, 3]. An excellent review of oblique wing history is given by Hirschberg et al.[4, 5] and a helpful introduction to oblique flying wings and their conceptual design is provided by Desktop Aeronautics. The advantage of oblique flying wings is that the sweep angle can be varied during a flight mission for different Mach numbers to obtain a high aspect ratio at low speeds and a low aspect ratio at high speeds[3, 5, 4]. Such performance is appealing for supersonic airplane design.

However, there are some difficulties with oblique flying wing or oblique all wing (OAW) concepts. For example, the configuration of an OFW is asymmetric about flight direction. The asymmetry of the configuration may create serious problems for stability and control, in particular at a high sweep angle[6, 7, 8, 9, 10]. Even though the modern fly-by-wire control system could significantly improve stability, it may come with increased trimmed drag penalty. All flying animals have symmetric bodies about the flight direction, which is an evolution of natural selection in an extremely long process. Second, to accommodate sufficient headroom for passengers, the airfoil thickness must be high and the OFW airplane size will be usually very large. This is because an OFW stacks the airfoil to align with the low speed flight direction in order to form a high aspect ratio elliptic planform. Hence, the airfoil chord is short. This is different from the regular flying wing concept that has the airfoil aligned with the cruise flight direction so that a long chord length can be used. The high thickness airfoil of an OFW would not be favorable for supersonic flight since it creates large wave drag. The large airplane size would also create airport operating difficulties[11]. Nonetheless, even though the oblique wing configuration has potential to achieve high aerodynamic efficiency, it does not have an inherent advantage in reducing sonic boom.

To minimize sonic boom, there are in general two strategies: The first strategy is to implement nose bluntness following the area rule suggested by Jones, Seebass, and George[12, 2, 13, 14]. A blunt nose design creates a shock distribution in which the greatest shock strengths are near the aircraft and the shocks are weakened gradually due to interaction with expansion waves as the shock waves travel from the aircraft to the ground. Unfortunately, this design also induces substantial wave drag since the entropy increase due to the strong shock waves is irreversible. The second strategy is to use a sharp nose in order to generate weak shock or isentropic compression to minimize or cancel shock waves and sonic boom. The sharp nose strategy is aerodynamically efficient but may produce a strong shock at mid-field and far-field distances from the aircraft. The conventional tube-wing configuration has difficulties in achieving isentropic compression since the fuselage is almost always formed by convex shape that will generate expansion waves as well as shock waves. In principle, a sharp nose with isentropic compression is more likely to achieve both high aerodynamic efficiency and low sonic boom than the nose bluntness method. The question is how to implement it. Darden investigated nose-blunt relaxation as a compromise between the blunt nosed low-boom aircraft and sharp nosed low drag design[15]. McLean found that the pressure signature that reaches the ground

from a long slender aircraft with minimal weight change may not fully develop into the far-field N-wave form[16].

The Quiet Supersonic Platform (QSP) program sponsored by DARPA made a remarkable progress in weakening the sonic boom of a conventional supersonic aircraft with tube-wing configuration[14]. The flight tests of F-5E aircraft with the nose bluntness reshaped by Northrop Grumman based on the area distribution rule suggested by George and Seebass in the 1960s shows a significant reduction of sonic boom strength[17]. However, the QSP program did not address high wave drag issue of supersonic flight.

The Quiet Spike^{TM} of Gulfstream Aerospace is a joint program with NASA Dryden Flight Research Center in which the concept of an extendable nose spike for sonic boom minimization was investigated[18]. In supersonic flight tests with a spike mounted on F-15B aircraft, the typical N-shaped pressure wave was reduced to a series of weaker shocks. However, the long spike brings structural difficulties to make it stable and results in other system complication and weight penalty. The Quiet Spike^{TM} concept may be feasible for a small business jet with 8-12 passengers. For a large supersonic transport, the feasibility of using such a long spike is uncertain.

For the Gulfstream Quiet Spike^{TM} configuration, a movable wing configuration is considered to reduce the sweep angle and increase aspect ratio at low speed takeoff and landing similar to the system of F-14. However, such a system to control the movable wing will bring severe weight penalty for the cruise efficiency. Overall, the Gulfstream Quiet Spike^{TM} is still limited to the conventional tube-wing configurations, which have the inherent difficulty of sonic boom, wave drag and volume requirement.

Aforementioned efforts have mostly focused on either reducing sonic boom or improving aerodynamic efficiency for supersonic airplane systems. So far, there is no viable aerodynamic system concept for supersonic airplanes that can achieve both high aerodynamic efficiency and low sonic boom. High aerodynamic efficiency has no warranty for low sonic boom[19].

Zha[20, 21, 22] has recently suggested a novel supersonic bi-directional flying wing concept (SBiDir-FW) aimed at achieving low sonic boom, minimizing wave drag, and improving subsonic performance. The SBiDir-FW concept is to combine the advantages of conventional symmetric airplane configurations for stability and variable sweep of oblique wing for high aerodynamic efficiency. In addition, the SBiDir-FW adopts an isentropic compression pressure surface to avoid or minimize shock generation and sonic boom. It employs sharp leading edge to aim at high aerodynamic efficiency and low sonic boom at the same time.

2 The Novel Concept: Supersonic Bi-Directional Flying Wing

The Supersonic Bi-Directional Flying Wing [20, 21, 22] is aimed at breaking through the technical barriers of high sonic boom, poor subsonic performance, and high wave drag of conventional supersonic tube-wing configurations. The SBiDir-FW concept includes the following features:

1) To achieve high aerodynamic efficiency for both supersonic and subsonic, the airplane is a flying wing or blended wing-body configuration with a symmetric planform about both the longitudinal and span axes with two flight directions altered by 90°. At subsonic flight, the planform will rotate 90° from the supersonic mode shown in Fig. 1 to the subsonic mode as shown in Fig. 2. Fig. 3 shows the 3D supersonic flight direction and the thin airfoil highlighted to form the flying wing to achieve low wave drag. Fig. 4 shows the subsonic mode after 90° rotation from the supersonic mode also with the subsonic airfoil highlighted. A reversed rotation will be done when the mode is changed

from subsonic to supersonic. Since the span is significantly shorter than the length, the subsonic airfoil will be significantly thicker than the supersonic airfoil as shown in Fig. 4 to provide high lift coefficient needed for subsonic flight. The aspect ratio at subsonic will be substantially increased to $(L/b)^2$ times of the supersonic aspect ratio, where L is the airplane length and b is the span. The sweep angle at subsonic will be largely reduced to 90° - Γ, where Γ is the sweep angle at supersonic mode. The conflict of subsonic and supersonic aerodynamic performance of conventional tube-wing configuration is hence removed. In other words, high supersonic aerodynamic performance will be naturally translated to high subsonic performance. The symmetric planform will let the trailing edge become leading during the rotation and generate lift to stabilize the mode transition similar to a flying Frisbee. The yaw moment to rotate the airframe will be generated by ailerons or flaps on the two sides of the flying wing. No powered driving system like that for swing wing is needed to rotate the airframe and hence the weight penalty and system complication can be avoided. The desirable transition mode Mach number is high subsonic such as about 0.8 to avoid the unsteady force introduced by shock waves at supersonic. Even though a thin airfoil is used to stack the flying wing in the supersonic direction, sufficient volume can be easily achieved due to the long length of the flying wing body, which is also the chord of the flying wing airfoil.

2) The other important purpose of SBiDir-FW is to avoid or minimize downward shock and hence sonic boom by employing an isentropic compression pressure surface. As the proof of concept at zero angle of attack, the SBiDir-FW example configuration in this paper has a flat pressure surface as shown by the highlighted airfoil in Fig. 3 and 4, which is the isentropic compression surface for AoA of zero. At a non-zero AoA, an concave isentropic compression surface will be designed to remove or minimize the downward shock wave and sonic boom. A 2D supersonic airfoil such as the one shown in Fig. 3 will generate a slightly negative lift at zero AoA. However, a 3D swept wing with leading edge sweep angle greater than the Mach cone angle will reduce the effective Mach number to subsonic and generate the surface pressure distribution similar to an subsonic airfoil[23], which will generate positive lift.

3) The sharp airfoil leading edge (LE) suggested for the SBiDir-FW may have small LE stall angle of attack. There may be three ways to increase the LE stall margin: 1)a conventional slat system to increase LE radius can be still used at takeoff and landing as shown in Fig. 5. 2) To avoid bringing a weight penalty of the slat system to the cruise mission, an active flow control method using radial flow injection at leading edge may be used to increase the stall margin for the sharp LE as shown in Fig. 6. This LE flow control is based on the theory that a virtual blunt body flow can be generated by superimposing a uniform flow with a source flow as illustrated in Fig. 7. A virtual round LE may be created by this flow control. This flow control concept is not proved yet and needs to be studied. 3) The stall margin and lift may be increased by making use of the Delta Wing type detached vortices from the leading edge of the airplane when taking-off and landing at high AoA as shown in Fig. 8.

4) Removing the non-lifting conical fuselage will provide the maximum flexibility to design optimal aerodynamic configuration such as the isentropic compression pressure surface. The large surface area of a SbiDir-FW will have low wing loading. With high aspect ratio at subsonic and hence higher maximum lift coefficient, the take-off and landing distance is expected to be significantly shorter than conventional supersonic airplane. To have sufficient headroom from the thin airfoil, the concept is very suitable for an airplane to hold large number of passengers and pay load to have a long length. For a small scale airplane, the blended wing-body with thicker airfoil in the middle to provide sufficient headroom could be used. The advantages of SBiDir-FW concept are also applicable to hypersonic flight.

3 Proof of Concept

Conceptually, the 90° rotation of mode transition will favor aerodynamic efficiency at both supersonic and subsonic. Even though optimizing the aerodynamic efficiency is challenging, achieving low sonic boom has been a more difficult task. This paper hence is focused on proving the concept that a SBiDir-FW configuration can avoid or minimize downward shock and hence sonic boom by adopting an isentropic compression pressure surface. The case studied in this paper as the proof of concept is a flight condition at AoA=0° for its simplicity since an isentropic compression surface at AoA=0° is a flat surface. For AoA of non-zero value, an isentropic compression surface may be designed using characteristic method.

3.1 Validation of Sonic Boom Simulation

As the first step, it is necessary to validate our sonic boom simulation tools. Simulation of sonic boom using CFD needs to emphasize on the off body phenomenon, which has different mesh requirement from predicting aerodynamic forces of an airplane[24]. The cone Model 1 in the NASA sonic boom wind tunnel testing[25] is used to validate the CFD mesh setup and numerical schemes selection. The half cone angle is 3.24°, the cone length is 2inch. The tested Mach numbers 2.01 is calculated numerically for its near field sonic boom signature. The computed results are compared with the experiment[25] and the CFD results of Wintzer et al[26]. The far field sonic boom signature is extrapolated using the NASA *NF Boom* code [27] based on the method of Thomas[28].

The in house FASIP(Flow-Acoustics-Structural Interaction Package) CFD code is used for the simulation. FASIP has been intensively validated for various 2D and 3D steady and unsteady flows. FASIP has implemented advanced numerical algorithms including various approximate Riemann solvers[29, 30, 31], 3rd order MUSCL schemes, high order WENO schemes and central differencing schemes[32, 33, 34, 35], non-reflective boundary conditions[36], implicit unfactored Gauss-Seidel dual time stepping for unsteady calculation[37, 38], fluid-structural interaction[39, 40, 41], Reynolds averaged Navier-Stokes turbulence models[42, 43], DES and LES[44, 45, 46, 47], preconditioning for incompressible flows[48, 35], and high scalability parallel computing[49]. For the sonic boom calculation in this paper, the Roe's approximate Riemann solver [50] with 3rd order MUSCL scheme[51] and Minmod limiter is used.

The cone Model 1[25] is simulated with full geometry and a cross section of the mesh is shown in Fig. 9. The mesh is inclined at the Mach angle to resolve the oblique shock waves. The computational domain size is extended one chord upstream, two and a half chords above and below the cone, and four and half chords downstream of the cone. The inlet boundary conditions is to fix all the variables at the freestresm conditions. The upper, lower, and downstream conditions are zero gradient extrapolation. As the initial trails, the RANS model with Baldwin-Lomax model was used and the near field sonic boom was significantly over-predicted due to the boundary layer thickness. The calculation is then switched to inviscid calculation as the methods used by other groups[24, 26, 52, 53]. For our CFD solver, the inviscid calculation is conducted with Reynolds number set to 10^{16} in the Navier-Stokes solver and slip wall boundary conditions enforced. The rear part of the cone with constant radius cylinder is extended to the exit boundary for the simplicity of boundary condition treatment. The baseline mesh is $181 \times 141 \times 61$ in the streamwise, radial and circumferential direction respectively.

Fig. 10 is the near field pressure signature at $H/L = 2$, where H is the vertical distance from the cone leading edge and L is the cone length. Fig. 10 shows that the present computed pressure signature agrees excellently with the computed results from [26], which has been validated with experiment. Fig. 11 is the extrapolation to $H/L = 10$ using the NASA *NF Boom* code[27] and

excellent agreement with the experimental measurement is achieved. Fig. 12 is the pressure contours of the cone Model 1 at incoming Mach number of 2.01. Fig. 13 is the mesh refinement results and shows that the over pressure signatures are identical with different sizes of meshes. It indicates that the over pressure signature computed using the baseline mesh is converged. The same numerical strategy validated for the NASA cone sonic boom results is used to simulate the following SbiDir-FW configuration.

3.2 Sonic Boom Analysis of a SbiDir-FW configuration, M=1.6

As the proof of concept, the SBiDir flying wing concept is used for a conceptual design of a supersonic civil transport with cruise Mach number of 1.6, payload of 70 passengers, and range of 2500 nautical miles at cruise altitude of 60,000ft[54]. The airfoil used is 3% thickness. The compound sweep is composed of two sweep angles of 80° and 60°. The length is 60m. The aspect ratio at supersonic is 1.04 and at subsonic is 7.28. The configuration looks similar to the one shown in Fig. 3. The Mach number of 1.6 is selected since there are several exisiting designs for supersonic business jest from other groups[18, 52, 53], which could be used as reference to compare the sonic boom level.

Half of the SbiDir-FW configuration is calculated due to the symmetry of the geometry. Fig. 14 shows the 3D mesh topology with 1 body length upstream of the aircraft leading edge, 2.5 lengths at the lower and upper boundary, 8 body lengths downstream of the trailing edge, and 4 body lengths in the span wise direction. The baseline mesh size is $161 \times 161 \times 61$ in the streamwise, vertical and spanwise direction respectively. Fig. 15 shows the upper surface mesh.

Fig. 16 shows the isentropic Mach number on the upper surface, which indicates a clear upward shock near the trailing edge of the flying wing. Fig. 17 is the isentropic Mach number on the lower surface, which shows that the pressure is fairly uniform in most of the area. However, there is a shock wave along the leading edge on the lower surface. When the AoA is increased to 2° as shown in Figs.18 and 19, the upper surface acceleration is more due to the higher flow turning. On the lower surface, the leading edge shock wave disappears and the pressure is more uniform than at zero AoA.

Fig. 20 shows the ratio of lift to pressure drag (wave drag) of the 3D SBiDir-FW compared with the 2D 3% airfoil used to form the SBiDir-FW. At AoA equal to zero, the SbiDir-FW achieves L/D_p of 5.3, whereas the 2D airfoil has a negative L/D_p. The positive lift of the SBiDir-FW at zero AoA is attributed to the large sweep angle, which reduces the effective Mach number to subsonic. Fig. 21 gives the values of the lift and drag coefficients vs AoA. Fig. 21 shows that the aerodynamic efficiency of the 3D SbiDir-FW reaches peak at AoA=2°. The overall aerodynamic efficiency of the 3D SbiDir-FW is significantly better than the 2D airfoil even though the 2D airfoil has no induced drag.

Fig. 22 is the near field over pressure signature at the location two body lengths below the aircraft. It shows that the pressure rise at AoA=0° is gradual and smooth due to the flat isentropic compression pressure surface. At higher AoA, the leading edge and trailing edge shock waves are stronger. Fig. 23 is the ground sonic boom signature extrapolated by using NASA *NF Boom* code[27] with the ground reflection factor of 1.9. At AoA=0°, the ground sonic boom signature preserves the near field pressure signature shape, which is in a shape of *sin* wave with smooth variation, whereas all other AoAs form the typical N-waves with two shock waves pulses. This is expected since the flat pressure surface does not create isentropic compression at $AoA \neq 0°$. The peak of the over pressure value at AoA=0° is 0.3psf, which was set as the challenging target goal of the DARPA QSP program and has been hardly met by the current state of the art[18, 52, 53].

Fig. 25 is the Mach number contours at 0%span (mid-plane). At the leading edge, the downward wave is basically an acoustics wave at the angle of Mach cone. The suction surface also has a very weak shock wave at the leading edge due to the sharp and thin airfoil. The weak front shock wave is desirable to minimize wave drag. The flow accelerates on the suction surface and forms a tail shock near trailing edge to restore the pressure to ambient value. On the pressure surface, the flow is expanded a little near trailing edge, but does not vary much overall. However, this does not prevent the significant pressure variation in the lower off body region such as the near field or far field due to the 3D effect. In other words, the pressure variation on the upper surface will propagate downward and create the over pressure signature in the near field and ground as shown in Figs. 22 and 23.

Fig. 26 is the Mach number contours at 75%span section. Due to the sweep effect, the airfoil section is behind the compression waves or bow shock generated by the airplane leading edge. Even though the freestream flow is at AoA=0°, the airfoil section at outer span actually experiences a slight negative AoA due to the downward compression waves and bow shock from the LE of the airplane. The negative AoA causes expansion waves at leading edge on the pressure surface in the outer span. Due to this reason, it may be helpful to twist the airfoil along span to align with the flow angle to create isentropic compression and further increase lift coefficient at AoA=0°.

Figs. 27 and 28 are the Mach number contours at 0% and 75% span sections at AoA=2°. The flow pattern at the 0% span section is not very different from the one at AoA=0°, but the acceleration on the suction is more due to the higher AoA. At the 75% span section, the leading edge expansion on the pressure surface disappears due to the higher AoA. This certainly contributes to the higher lift coefficient as displayed in Fig. 21. It needs to be investigated if it also contributes to the sonic boom increase as shown in Figs. 22 and 23.

Figs. 29, 30, 31, and 32 are the surface Mach number distributions at 0%, 25%, 50% and 75% span. These plots clearly show that at AoA=0°, there is a strong expansion/compression at leading edge of the pressure surface at the outer span location as explained for Fig. 26 due to the negative AoA.

To demonstrate the 3D effect of the upper surface pressure variation on the lower off body region, Figs. 33 and 34 show the Mach contours at AoA=0° at 50% streamwise location and near trailing edge of the airplane. Fig. 33 shows that at the mid-streamwise location, the upper surface gradient affects the lower surface primarily in the wing tip region due to the maximum wind span. Near the trailing edge as shown by Fig. 34, the lower off body region is strongly affected by the upper off body gradient. Figs. 35 and 36 are the Mach number contours for AoA=1° at the same streamwise location. The conclusion of the 3D effect is similar to the case of AoA=0°. This 3D effect phenomenon means that when the downward sonic boom is minimized, both the lower surface and upper surface wave structures need to be considered.

3.3 Comments

The smooth ground sonic boom signature with 0.3psf at AoA=0° as shown in Fig. 23 indicates that it is indeed possible to achieve no sonic boom by using the flying wing concept with isentropic compression on the pressure surface. However, the configuration studied in this paper does not include the engine effect, which will negatively affect the sonic boom performance even though they are installed on the upper side. At the same time, this configuration is created with no optimization at all with the purpose only to demonstrate the concept. Our simulation indicates that the sonic boom is affected by several factors including sweep angle, aspect ratio, angle of attack, twist of airfoil in span, upper surface spanwise shape, etc. The SbiDir-FW configuration created using our geometry

model is also not smooth as can be seen in Fig. 3 and 4 due to time and man power constraints. In other words, there is large room to further improve both the aerodynamic efficiency and sonic boom performance. Compared with the various supersonic tube-wing configurations with no engines installed tested in [19], the sonic boom of the current configuration with the lift coefficient even at the non-isentropic compression AoA of 1° and 2° is superior.

4 Conclusions

This paper introduces a novel concept of supersonic bi-directional flying wing, which is to achieve low sonic boom, low supersonic wave drag, and high subsonic performance. The SBiDir-FW planform is symmetric about both longitudinal and span axes. For supersonic flight, the planform is designed to achieve optimum aspect ratio, span, and sweep angle to minimize wave drag. For subsonic mode, the airplane will rotate 90° and the sweep angle of the LE at subsonic mode is hence significantly reduced and the aspect ratio is substantially increased by $(L/b)^2$, where L is the airplane length, and b is the span. This will allow the airplane to have high subsonic performance with short take-off and landing distance and low stall velocity due to low wing loading and high maximum lift coefficient. The airfoil suggested is symmetric about the 50% chord location with both sharp leading edge (LE) and sharp trailing edge (TE). To minimize or avoid sonic boom by canceling or weakening the downward shock wave, the pressure surface of the flying wing will employ a shape generating isentropic compression waves. At zero angle of attack (AoA), a flat pressure surface roughly achieves this purpose based on 2D theory. The proposed supersonic flying wing concept significantly simplifies a supersonic airplane configuration by removing the fuselage-wing interaction. It provides the maximum flexibility to design optimal aerodynamic configuration to satisfy aerodynamic efficiency and sonic boom. The SBiDir-FW platform combines the advantages of varying sweep angle of an oblique flying wing and the high stability of conventional symmetric flying wing configuration.

The CFD simulation conducted in this paper demonstrates that the SBiDir-FW configuration studied achieves low ground sonic boom at 0.3psf with $L/D_p = 5.3$ at AoA=0°. Furthermore, the ground pressure signature is not the typical N shape wave with two strong shock wave pulses, but is in a smooth *sin* wave shape. This indicates that it is indeed possible to cancel sonic boom by SBiDir-FW configuration. For the example SbiDir-FW configuration studied in this paper, when the AoA is increased to 1° or 2°, the L/D_p as well as the sonic boom are significantly increased as expected. Future work will be focused on optimizing the SBiDir-FW concept including isentropic compression pressure surface at non-zero AoA, aspect ratio, sweep angle, spanwise airfoil twist, planform shape, upper surface spanwise shape, airfoil shape, etc in order to achieve minimal or zero sonic boom with optimal aerodynamic efficiency.

5 Acknowledgment

We greatly appreciate the grant support from Florida Center for Advanced Aero-Propulsion for this research. The discussion with Lou Cattafesta at Univ. of Florida, Farrukh Alvi at Florida State Univ., Harry Welge and Arvin Shmilovich at Boeing Company, and Jeffry Padin at The Aerospace Corporation is very helpful to guide this research. We also would like to thank Don Durston from NASA Ames Research Center for providing the NF Boom code. Our sincere thanks are also extended to Mathias Wintzer at Stanford University and Michael Aftosmis at NASA Ames Research Center for providing their CFD sonic boom results for our code validation. The computing resource support from the Center for Computational Sciences at University of Miami is greatly appreciated.

References

[1] Plotkin, K. J. and Maglieri, D. , " Sonic Boom Research: History and Future." AIAA 2003-3575, 23-26 June, 2003.

[2] Mack, R. J., and Needleman, K.E., "A Methodology for Designing Aircraft to Low Sonic Boom Constraints." NASA TM-4246, February 1991, 1991.

[3] Mack, R. J., and Needleman, K.E., "Aerodynamic Design for Supersonic Speeds." Proceedings of the 1st International Congress in the Aeronautical Sciences (ICAS), Advances in Aeronautical Sciences, Vol 1., Pergamon Press, NY,, 1959.

[4] Hirschberg, M., Hart, D. and Beutner, T., "A Summary Of A Half-Century of Oblique Wing Research." AIAA Paper 2007-150, 2007.

[5] Desktop Aeronautics, Inc., "Oblique Flying Wings: An Introduction and White Paper." http://www.desktopaero.com/obliquewing/library/whitepaper/index.html, 2005.

[6] Campbell, J.P., and Drake, H.M., "Investigation of stability and control characteristics of an airplane model with a skewed wing in the Langley free flight tunnel." NACA TN-1208, May 1947.

[7] Matthews, H. , "Oblique Wing Research Aircraft NASA AD-1." World X-Planes Magazine, No. 2, 2005.

[8] Kroo, I.M., "The Aerodynamic Design of Oblique Wing Aircraft." Proceedings of the AIAA/AHS/ASEE Aircraft Systems Design and Technology Meeting, CP 86-2624, AIAA, Washington D.C., 2005.

[9] Kennelly, R.A., Carmichael, R., Strong, J., and Kroo, I.M., "Transonic Wind Tunnel Test of a 14% Thick Oblique Wing." NASA TM-102230, Aug. 1990.

[10] Kempel, R.W., McNeill, W.E., and Maine, T.A., "Oblique-Wing Research Aircraft Motion Simulation with Decoupling Control Laws." AIAA Paper 88-402, 1988.

[11] R. Jones, " Technical Note - The Flying Wing Supersonic Transport ," *Aeronautical Journal*, vol. 3, March 1991.

[12] L. B. Jones, " Lower Bounds for Sonic Bangs ," *Journal of the Royal Aeronautical Society*, vol. 65, 606, pp. 433–436, 1961.

[13] R. Seebass and A. George, " Sonic-Boom Minimization ," *Journal of the Royal Aeronautical Society of America*, vol. 51, 2, pp. 686–694, 1972.

[14] Graham, D., "Quiet Supersonic Platform, Shaped Sonic Boom Demonstrator (SSBD) Program." FAA Civil Supersonic Aircraft Workshop, http://www.aee.faa.gov/Noise/aee100_files/SonicWkshp/2-Panel1-Graham-Northrop.pdf, Nov. 2003.

[15] Darden, C. M., "Sonic-Boom Minimization With Nose-Bluntness Relaxation." NASA TP-1348, January 1979.

[16] McLean, F. E., "Some Nonasymptotic Effects on the Sonic Boom of Large Airplanes." NASA TN D-2877, 1965.

[17] S. R. George, A.R., " Sonic Boom Minimization including Both Front and Rear Shocks ," *AIAA Journal*, vol. 9, 10, pp. 2091–2093, 1971.

[18] Howe, D., Simmons, F., and Freund, D., "Development of the Gulfstream Quiet SpikeTM for Sonic Boom Minimization." AIAA Paper 2008-124, 2008, 7-10, Jan. 2008.

[19] Hunton, L. W. and Mendoza, J. P. and Hicks, R. M., " Some Effects of Wing Planform on Sonic Boom." NASA TN D-7160, Jan 1973.

[20] Zha, G.-C., " Supersonic Flying Wing with Low Sonic Boom, Low Wave Drag, and High Subsonic Performance (SFW-L^2HSP)." Technology Transfer Office UMI-163, University of Miami,FL, Dec. 2008.

[21] Zha, G.-C., " Supersonic Bi-Directional Flying Wing." Provisional patent application No. 61172929, Submitted to USPTO, 27 Apr. 2009.

[22] Zha, G.-C., " Toward Zero Sonic-Boom and High Efficiency Supersonic UAS: A Novel Concept of Supersonic Bi-Directional Flying Wing." US Air Force Academic Outreach UAS Symposium, Grand Forks, ND, Aug. 4-6, 2009.

[23] L. Reithmaier, *Mach 1 and Beyond, The Illustrated Guide to High-Speed Flight.* TAB Books, a division of McGraw-Hill, Inc., 1995.

[24] Casper, J. H. and Cliff, S. E. and Thomas, S. D. and Park, M. A. and McMullen, M.S. and Melton, J. E. and Durston, D. A., " Assessment of Near-Field Sonic Boom Simulation Tools." AIAA Paper 2008-6592, 26th AIAA Applied Aerodynamics Conference, Honolulu, Hawaii, 18-21 Aug. 2008.

[25] Carlson, H. W. and Mack, R.J. and Morris, O. A. , " A Wind Tunnel Investigation of the Effect of Body Shape on Sonic Boom Pressure Distribution." NASA TN-D-3106, Nov. 1965.

[26] Wintzer, M. and Nemec, M. and Aftosmis, M. J., " Adjoint-Based Adaptive Mesh Refinement for Sonic Boom Prediction." AIAA 2008-6593, 26th AIAA Applied Aerodynamics Conference, Honolulu, Hawaii, 18-21 Aug. 2008.

[27] Durston, D. A. , " Sonic Boom Extrapolation and Sound Level Prediction." Unpublished Document, NASA Ames Research Center, Sept. 2009.

[28] Thomas, C. L., " Extrapolation of Sonic Boom Pressure Signatures by the Waveform Parameter Method." NASA TN D-6832, June 1972.

[29] G.-C. Zha, Y. Shen, and B. Wang, "Calculation of Transonic Flows Using WENO Method with a Low Diffusion E-CUSP Upwind Scheme." AIAA Paper 2008-0745, 46th AIAA Aerospace Sciences Meeting, Reno, NV, Jan. 2008.

[30] G.-C. Zha, "Low Diffusion Efficient Upwind Scheme ," *AIAA Journal*, vol. 43, 2005.

[31] G.-C. Zha and Z.-J. Hu, "Calculation of Transonic Internal Flows Using an Efficient High Resolution Upwind Scheme," *AIAA Journal*, vol. 42, No. 2, pp. 205–214, 2004.

[32] Shen, Y.-Q. and Zha, G.-C. , " Improvement of the WENO Scheme Smoothness Estimator," *International Journal for Numerical Methods in Fluids*, vol. DOI:10.1002/fld.2186, 2009.

[33] Shen, Y.-Q. and Zha, G.-C. and Chen, X.-Y., " High Order Conservative Differencing for Viscous Terms and the Application to Vortex-Induced Vibration Flows," *Journal of Computational Physics*, vol. 228(2), pp. 8283–8300, 2009.

[34] Y.-Q. Shen, G.-C. Zha, and B.-Y. Wang, "Improvement of Stability and Accuracy of Implicit WENO Scheme ," *AIAA Journal*, vol. 47, pp. 331–344, 2009.

[35] Shen, Y.-Q. and Zha, G.-C., " Improved Seventh-Order WENO Scheme ." AIAA Paper 2010-1451, 48th AIAA Aerospace Sciences Meeting, Orlando, FL, Jan. 4-6, 2010.

[36] X. Chen and G.-C. Zha, "Implicit Application of Non-Reflective Boundary Conditions for Navier-Stokes Equations in Generalized Coordinates," *International Journal for Numerical Methods in Fluids*, vol. 50, 2006.

[37] Z.-J. Hu and G.-C. Zha, "Calculations of 3D Compressible Using an Efficient Low Diffusion Upwind Scheme," *International Journal for Numerical Methods in Fluids*, vol. 47, pp. 253–269, 2004.

[38] Y.-Q. Shen and G.-C. Zha, "A Comparison Study of Gauss-Seidel Iteration Methods for Internal and External Flows ." AIAA Paper 2007-4332, 2007.

[39] X.-Y. Chen, G.-C. Zha, and M.-T. Yang, "Numerical Simulation of 3-D Wing Flutter with Fully Coupled Fluid-Structural Interaction," *Journal of Computers & Fluids*, vol. 36, No. 5, pp. 856–867, 2007.

[40] X.-Y. Chen and G.-C. Zha, "Fully Coupled Fluid-Structural Interactions Using an Efficient High Resolution Upwind Scheme," *Journal of Fluids and Structures*, vol. 20, pp. 1105–1125, 2005.

[41] Wang, B. Y and Zha, G.-C., "High Fidelity Simulation of Nonlinear Fluid-Structural Interaction with Transonic Airfoil Limit Cycle Oscillations," *Accepted for publication in Journal of Fluids and Structures*, 2010.

[42] Wang, B.-Y. and Haddoukessouni, B. and Levy, J. and Zha, G.-C., "Numerical Investigations of Injection Slot Size Effect on the Performance of Co-Flow Jet Airfoil," *Journal of Aircraft*, To appear 2008.

[43] B. Wang and G.-C. Zha, "Comparison of a Low Diffusion E-CUSP and the Roe Scheme for RANS Calculation." AIAA Paper 2008-0596, 46th AIAA Aerospace Sciences Meeting and Exhibit, Jan. 7-10, 2008.

[44] Coronado, P. and Wang, B.-Y. and Zha, G.-C., " Delayed-Detached-Eddy Simulation of Shock Wave/Turbulent Boundary Layer Interaction ." AIAA Paper 2010-0109, 48th AIAA Aerospace Sciences Meeting, Orlando, FL, Jan. 4-6, 2010.

[45] Chen, X.-Y. and Wang, B.-Y. and Zha, G.-C. , "Detached Eddy Simulation of 3-D Wing Flutter with Fully Coupled Fluid-Structural Interaction." AIAA Paper 2010-0053, 48th AIAA Aerospace Sciences Meeting, Orlando, FL, Jan. 4-6, 2010.

[46] Y.-Q. Shen and G.-C. Zha, "Comparison of High Order Schemes for Large Eddy Simulation of Circular Cylinder Flow." AIAA-2009-0945, Submitted to Journal of Computational Physics, 2009.

[47] B. Wang and G. - C. Zha , " Detached Eddy Simulations of a Circular Cylinder Using a Low Diffusion E-CUSP and High-Order WENO Scheme." AIAA Paper 2008-3855, AIAA 38th Fluid Dynamics Conference, Seattle, Washington, June 23-26, 2008.

[48] Y.-Q. Shen and G.-C. Zha, "Simulation of Flows at All Speeds with WENO Scheme and Preconditioning." AIAA Paper 2009-1312, AIAA 47th Aerospace Sciences Meeting, Orlando, FL, Jan. 5-8, 2009.

[49] Wang, B.-Y. and Haddoukessouni, B. and Levy, J. and Zha, G.-C., "Numerical Investigations of Injection Slot Size Effect on the Performance of Co-Flow Jet Airfoil ," *AIAA Journal of Aircraft*, vol. 45, pp. 2084–2091, 2008.

[50] P. Roe, "Approximate Riemann Solvers, Parameter Vectors, and Difference Schemes," *Journal of Computational Physics*, vol. 43, pp. 357–372, 1981.

[51] B. Van Leer, "Towards the Ultimate Conservative Difference Scheme, III," *Journal of Computational Physics*, vol. 23, pp. 263–75, 1977.

[52] Ishikawa, H. and Makino, Y. and Ito, T. and Kuroda, F., " Sonic Boom Prediction Using Multi-Block Structured Grids CFD Code Considering Jet-On Effects." AIAA 2009-3508, June 2009.

[53] Choi, S. and Alonso, J. J. and Kroo, I. M. and Wintzer, M. , " Multi-Fidelity Design Optimization of Low Boom Supersonic Business Jets." AIAA 2004-4371, Aug. 30-Sept. 1, 2004.

[54] Espinal, D. and Im, H. and Lee, B. and Sposato, H. and Kinard, D. and Dominguez, J. and Zha, G.-C., " Supersonic Bi-Directional Flying Wing, Part II: Conceptual Design of A High Speed Civil Transport ." AIAA Paper 2010-1393, 48th AIAA Aerospace Sciences Meeting, Orlando, FL, Jan.4-6, 2010.

[55] A. V. Dyke, *An album of fluid motion.* Stanford: Parabolic Press, 1982.

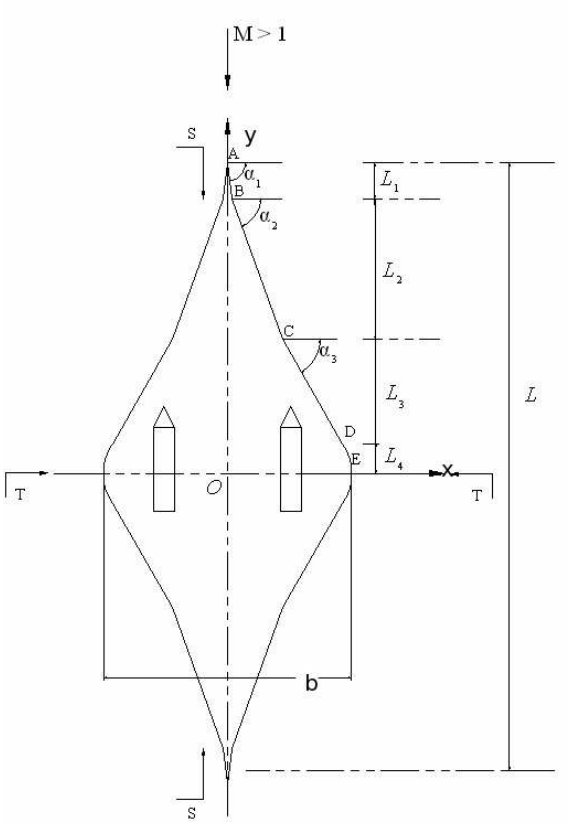

Figure 1: Sketch of a SBiDir-FW Planform flying in supersonic mode (not to scale)

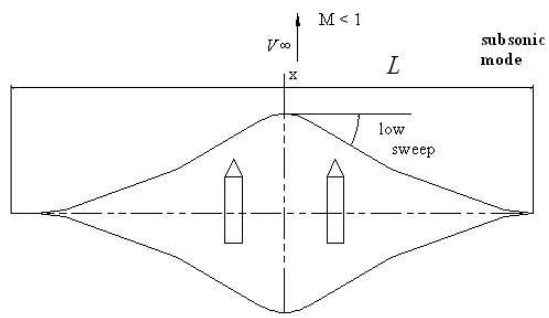

Figure 2: Sketch of a SBiDir-FW Planform flying in subsonic mode (not to scale)

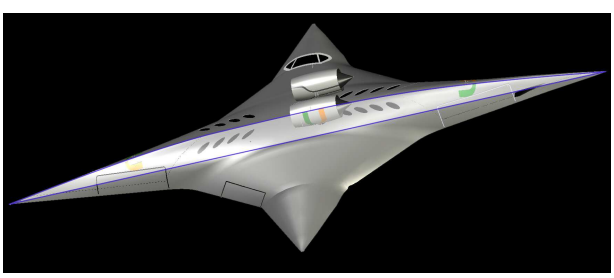

Figure 3: A SBiDir-FW civil transport in supersonic mode flying toward right, supersonic thin airfoil highlighted in the middle.

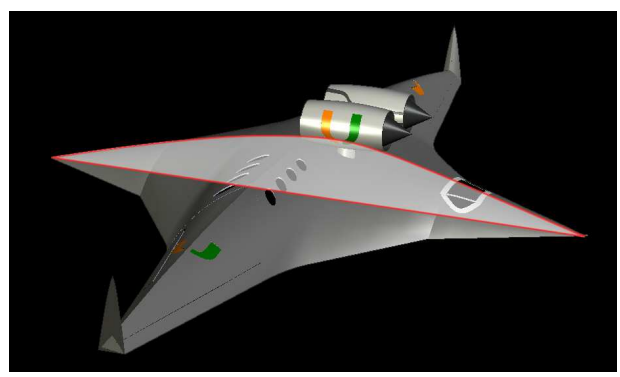

Figure 4: A SBiDir-FW civil transport in subsonic mode flying toward right, subsonic thick airfoil highlighted in the middle.

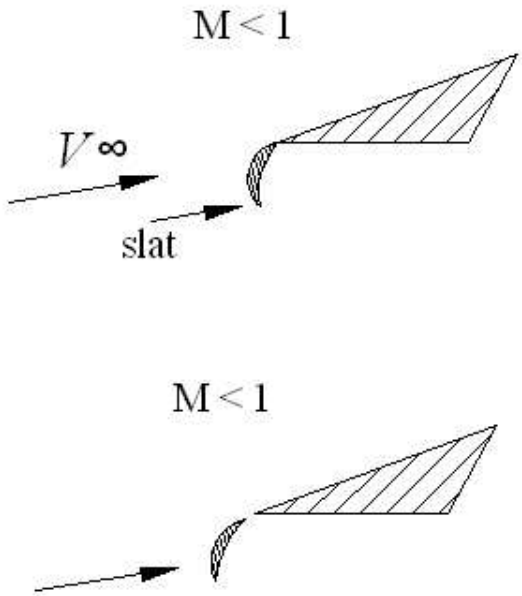

Figure 5: Using slats to increase stall margin of a sharp airfoil.

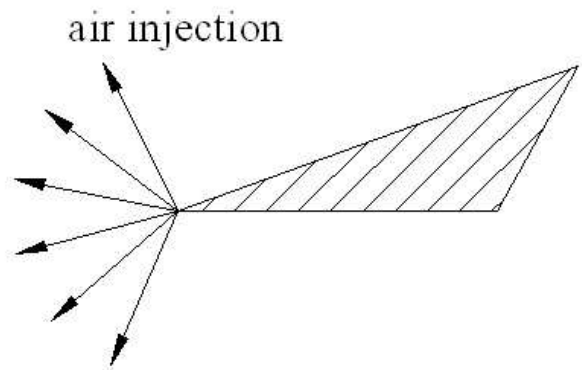

Figure 6: Using leading edge radial injection to increase stall margin of a sharp airfoil.

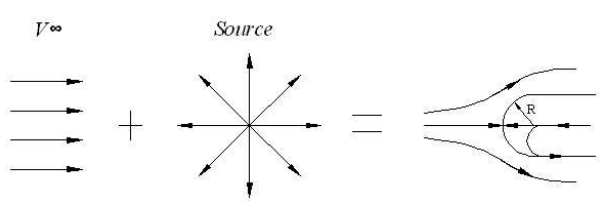

Figure 7: A uniform flow superimposed with a source flow to form a blunt body flow.

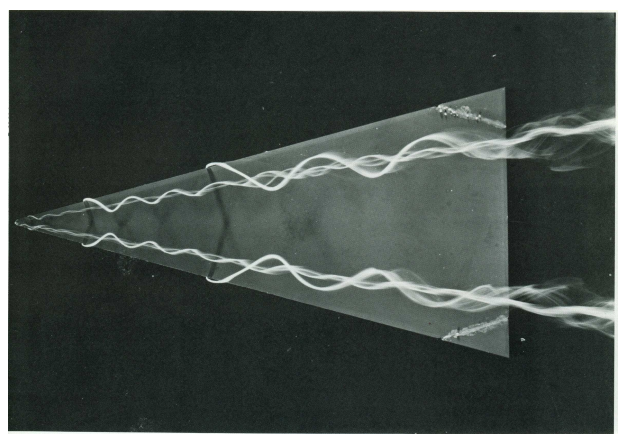

Figure 8: Lift enhancement by Delta wing leading edge vortices, image from [55]

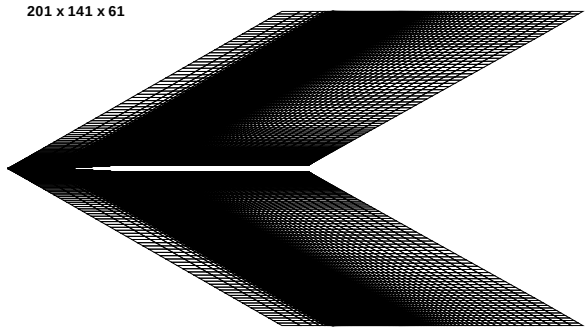

Figure 9: Cross section of the mesh for NASA cone Model 1[25].

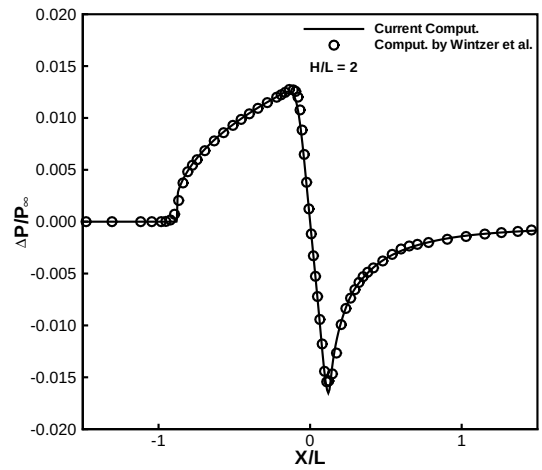

Figure 10: Computed Over-pressure at two body lengths below the cone Model 1 compared with the result from[26].

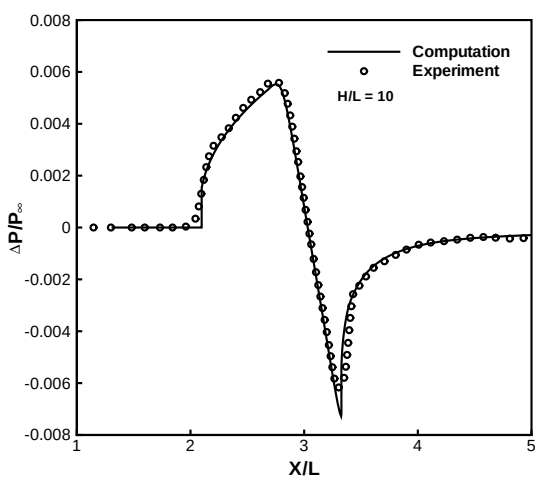

Figure 11: Computed Over-pressure at ten body lengths below the cone Model 1 compared with experiment[25].

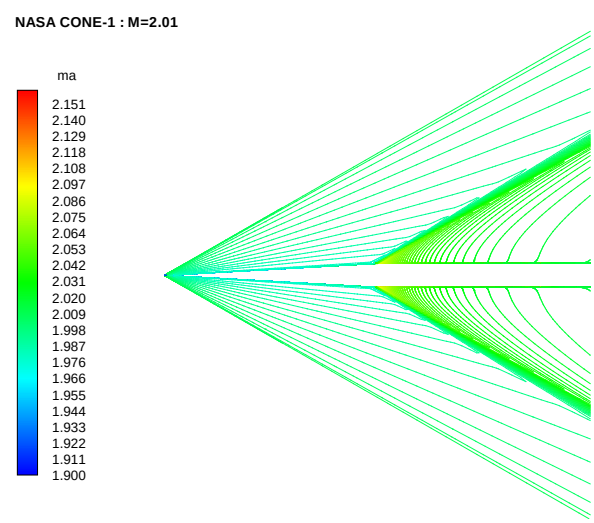

Figure 12: Computed pressure contours of the cone Model 1.

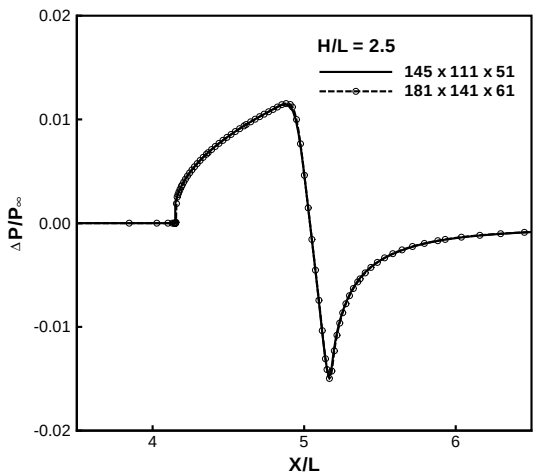

Figure 13: Comparison of the computed overpressure at two and half body lengths below the cone Model 1 for mesh refinement study.

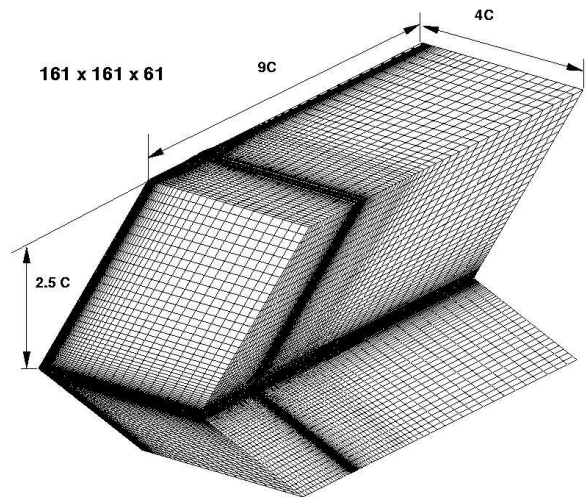

Figure 14: 3D mesh topology for the SbiDir-FW configuration.

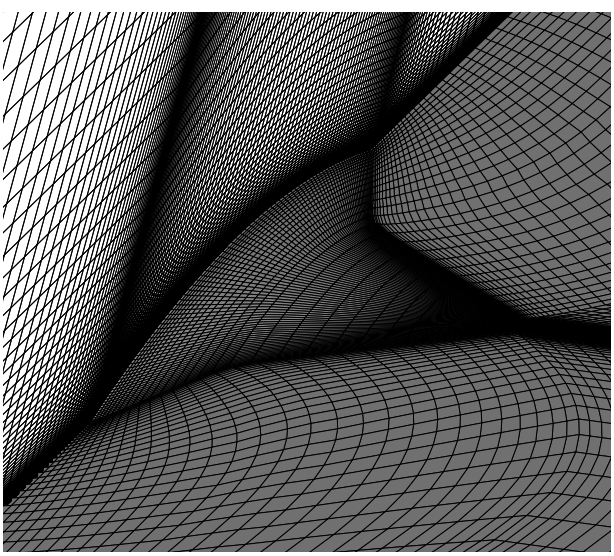

Figure 15: Surface mesh of the SbiDir-FW configuration.

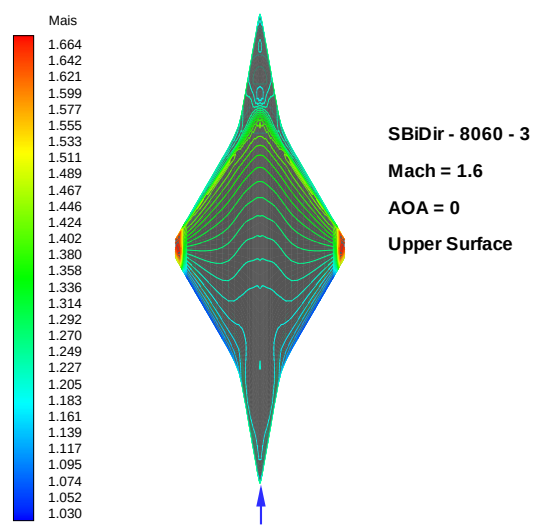

Figure 16: Computed isentropic Mach number contours at upper surface of a 3D SbiDir-FW, AoA=0°.

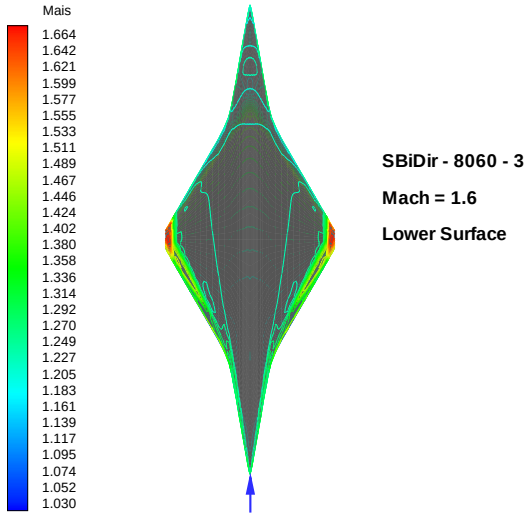

Figure 17: Computed isentropic Mach number contours at lower surface of a 3D SbiDir-FW, AoA=0°.

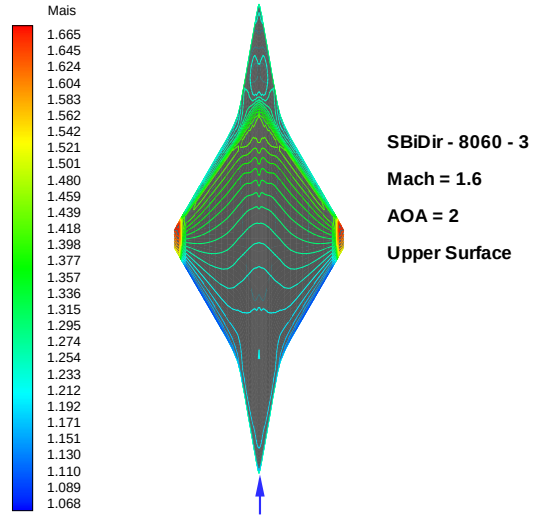

Figure 18: Computed isentropic Mach number contours at upper surface of a 3D SbiDir-FW, AoA=2°.

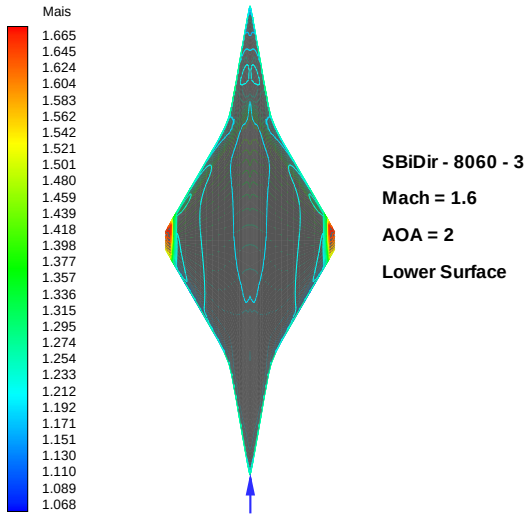

Figure 19: Computed isentropic Mach number contours at lower surface of a 3D SbiDir-FW, AoA=2°.

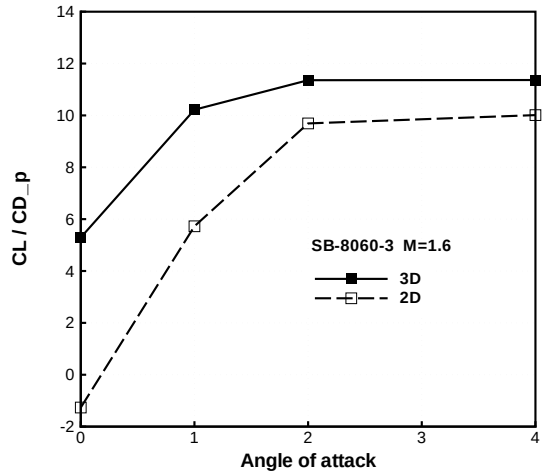

Figure 20: Computed lift to drag ratio vs AoA for the 3D SbiDir-FW and 2D 3% airfoil thickness.

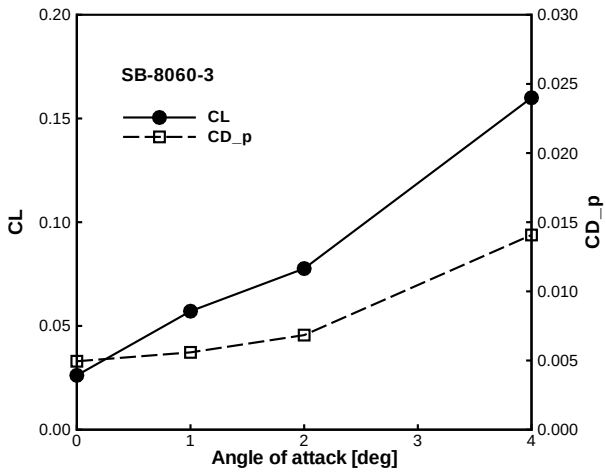

Figure 21: Computed lift and drag coefficient vs AoA for the 3D SbiDir-FW.

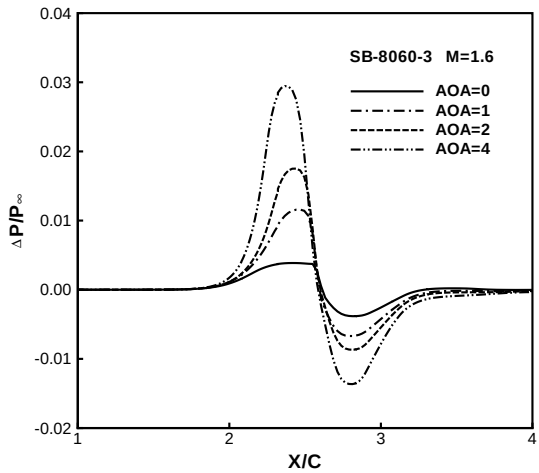

Figure 22: Computed near field pressure signature at two body lengths below.

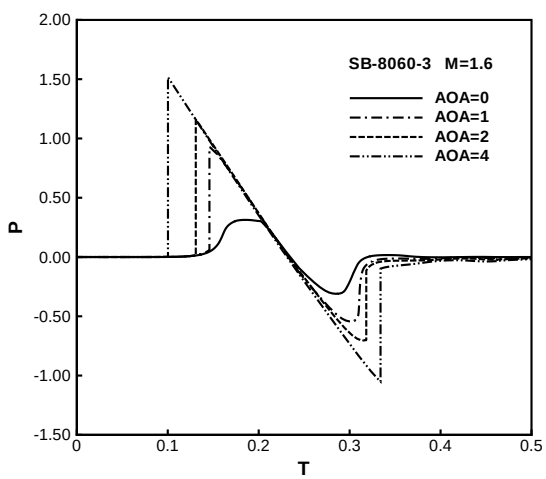

Figure 23: Computed sonic boom signature on ground.

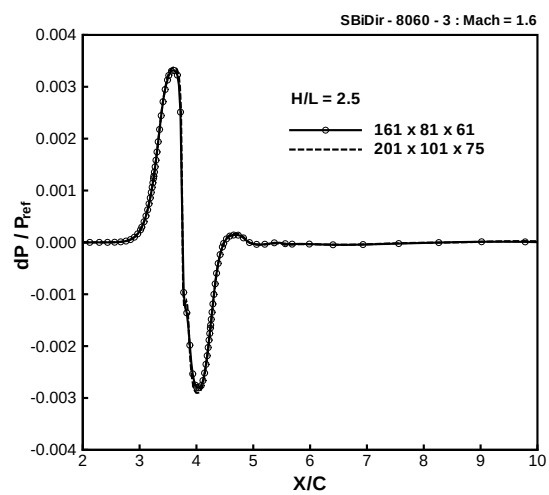

Figure 24: Mesh refinement results of the pressure signature for SbiDir-FW configuration

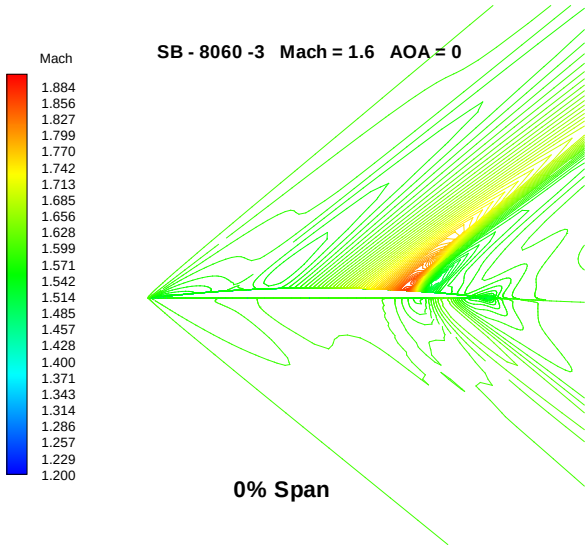

Figure 25: Mach number contours at 0% span section(mid-plane) and AoA=0°.

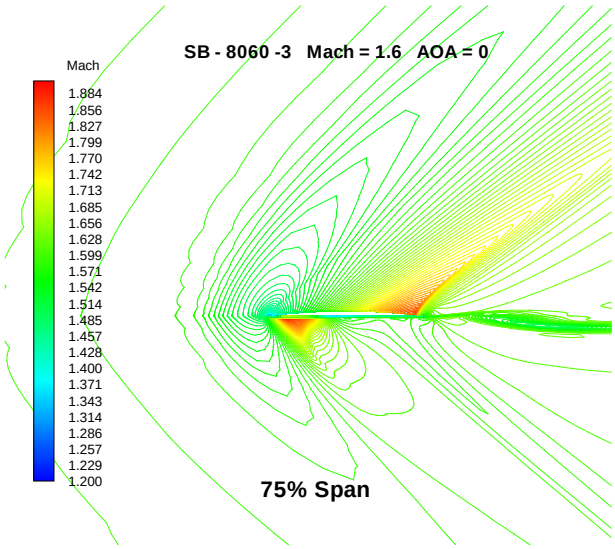

Figure 26: Mach number contours at 75% span section and AoA=0°.

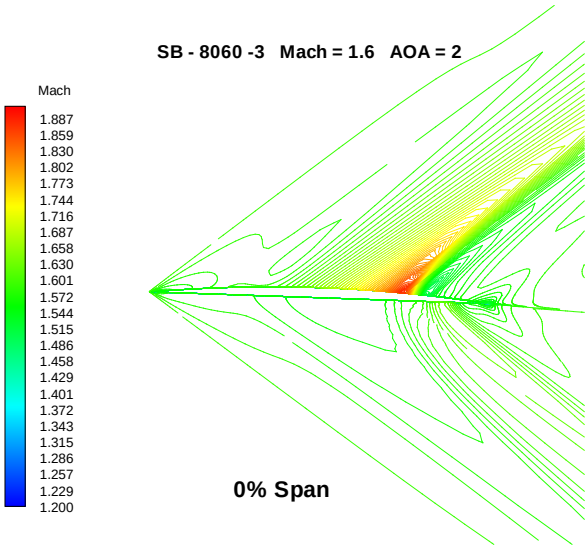

Figure 27: Mach number contours at 0% span section(mid-plane) and AoA=2°.

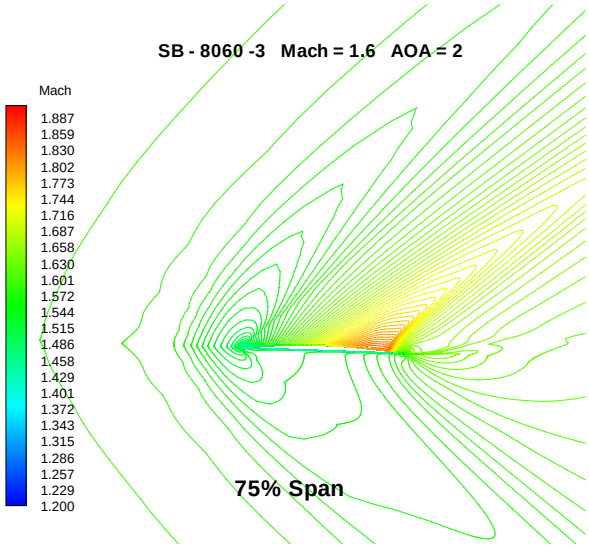

Figure 28: Mach number contours at 75% span section and AoA=2°.

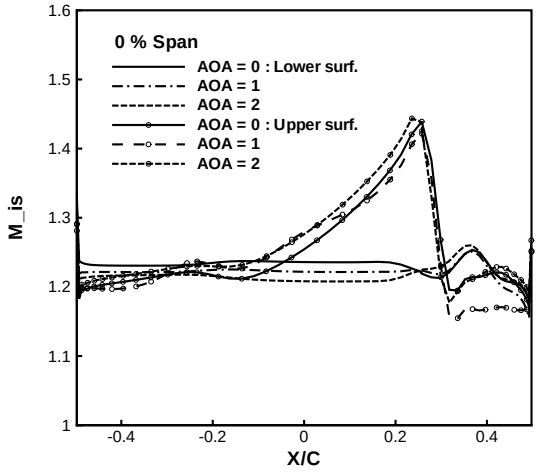

Figure 29: Surface Mach number distribution at 0% span section(mid-plane).

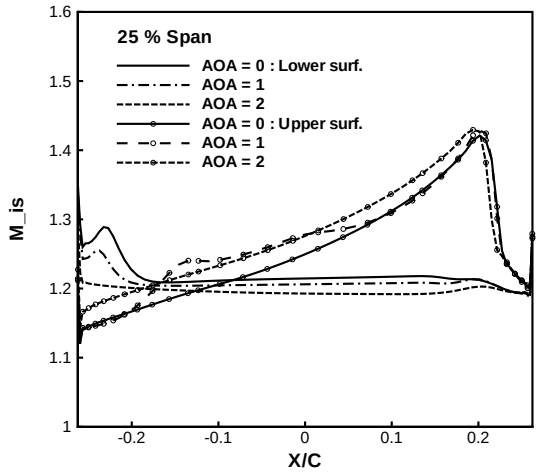

Figure 30: Surface Mach number distribution at 25% span section.

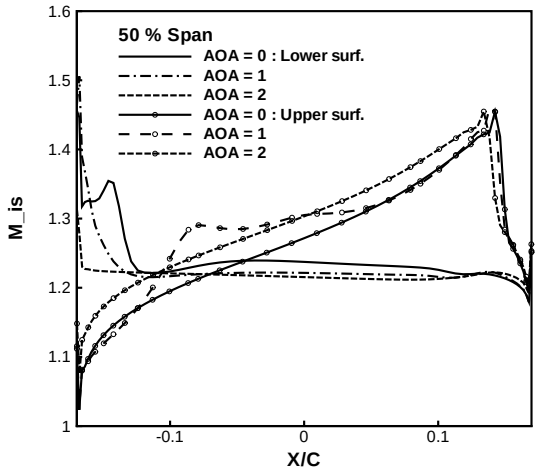

Figure 31: Surface Mach number distribution at 50% span section(mid-plane).

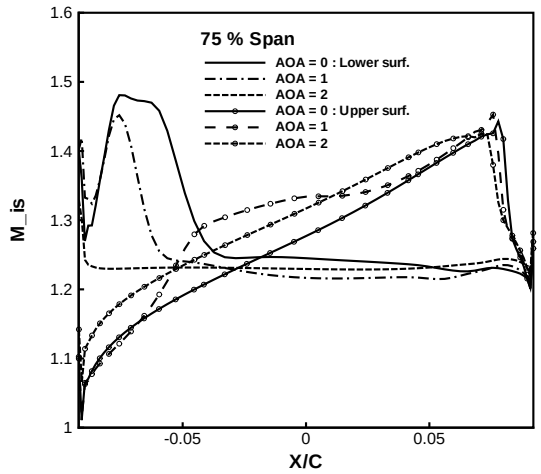

Figure 32: Surface Mach number distribution at 75% span section.

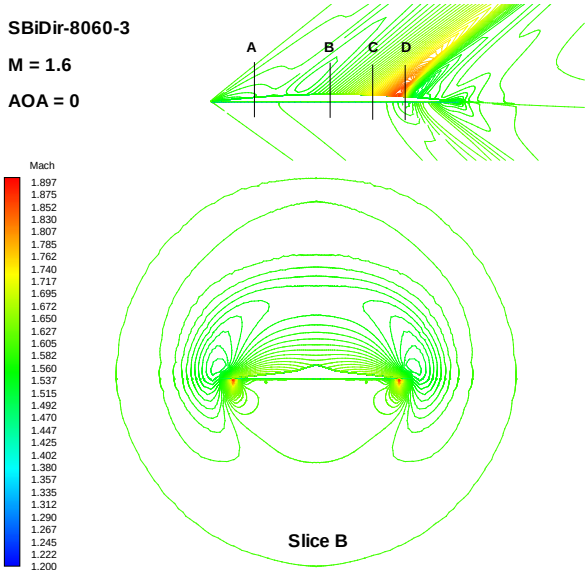

Figure 33: Mach number contours at cross section B, AoA=0°.

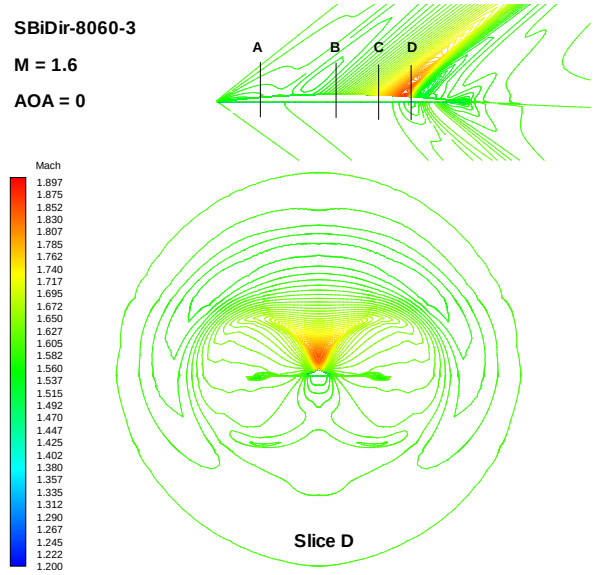

Figure 34: Mach number contours at cross section D, AoA=0°

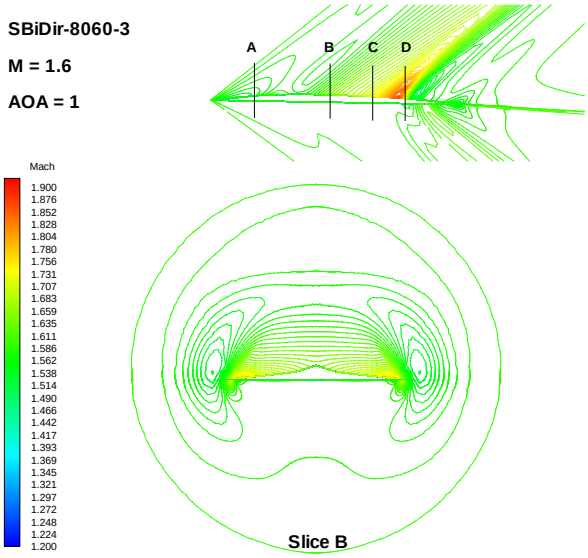

Figure 35: Mach number contours at cross section B, AoA=1°.

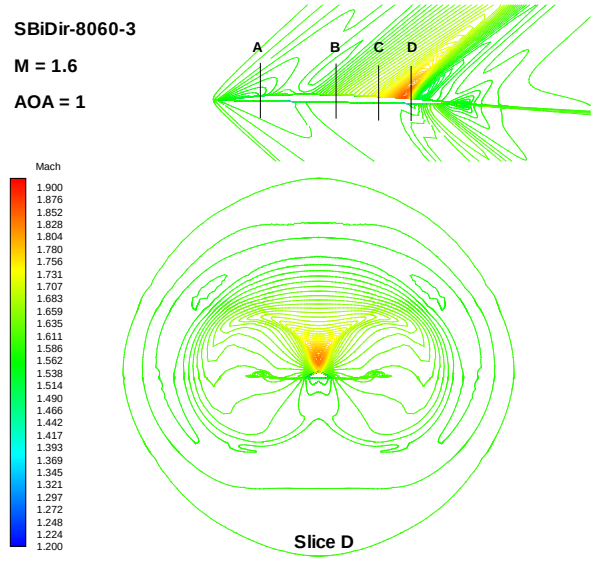

Figure 36: Mach number contours at cross section D, AoA=1°